Geochemistry Geophysics Geosystems G3
AN ELECTRONIC JOURNAL OF THE EARTH SCIENCES
Published by AGU and the Geochemical Society

Article
Volume 11, Number 3
11 March 2010
Q03007, doi:10.1029/2009GC002667
ISSN: 1525-2027

Volume change associated with formation and dissociation of hydrate in sediment

J. Y. Lee
Petroleum and Marine Resources Division, Korea Institute of Geoscience and Mineral Resources, 92 Gwahang-no, Yuseong-gu, Daejeon 305-350, South Korea (jyl@kigam.re.kr)

J. C. Santamarina
School of Civil and Environmental Engineering, Georgia Institute of Technology, 790 Atlantic Drive, Atlanta, Georgia 30332-0355, USA (jcs@gatech.edu)

C. Ruppel
U.S. Geological Survey, 384 Woods Hole Road, Woods Hole, Massachusetts 02543, USA (cruppel@usgs.gov)

[1] Gas hydrate formation and dissociation in sediments are accompanied by changes in the bulk volume of the sediment and can lead to changes in sediment properties, loss of integrity for boreholes, and possibly regional subsidence of the ground surface over areas where methane might be produced from gas hydrate in the future. Experiments on sand, silts, and clay subject to different effective stress and containing different saturations of hydrate formed from dissolved phase tetrahydrofuran are used to systematically investigate the impact of gas hydrate formation and dissociation on bulk sediment volume. Volume changes in low specific surface sediments (i.e., having a rigid sediment skeleton like sand) are much lower than those measured in high specific surface sediments (e.g., clay). Early hydrate formation is accompanied by contraction for all soils and most stress states in part because growing gas hydrate crystals buckle skeletal force chains. Dilation can occur at high hydrate saturations. Hydrate dissociation under drained, zero lateral strain conditions is always associated with some contraction, regardless of soil type, effective stress level, or hydrate saturation. Changes in void ratio during formation-dissociation decrease at high effective stress levels. The volumetric strain during dissociation under zero lateral strain scales with hydrate saturation and sediment compressibility. The volumetric strain during dissociation under high shear is a function of the initial volume average void ratio and the stress-dependent critical state void ratio of the sediment. Other contributions to volume reduction upon hydrate dissociation are related to segregated hydrate in lenses and nodules. For natural gas hydrates, some conditions (e.g., gas production driven by depressurization) might contribute to additional volume reduction by increasing the effective stress.

Components: 6885 words, 7 figures, 1 table.

Keywords: gas hydrate; hydrate-bearing sediment; phase transformation; strain.

Index Terms: 3004 Marine Geology and Geophysics: Gas and hydrate systems; 3022 Marine Geology and Geophysics: Marine sediments: processes and transport; 1823 Hydrology: Frozen ground; 5112 Physical Properties of Rocks: Microstructure.

Received 8 June 2009; **Revised** 4 December 2009; **Accepted** 17 December 2009; **Published** 11 March 2010.

Lee, J. Y., J. C. Santamarina, and C. Ruppel (2010), Volume change associated with formation and dissociation of hydrate in sediment, *Geochem. Geophys. Geosyst.*, *11*, Q03007, doi:10.1029/2009GC002667.

1. Introduction

[2] Gas hydrate forms when the constituents (water and hydrate-forming low molecular weight gas) are present in the required amounts at a suitable range of low temperatures, moderate pressures, and appropriate pore water and soil conditions. Temperature, pressure, or pore water perturbations that take gas hydrate outside its thermodynamic stability field lead to its dissociation. Until recently, gas hydrate formation and dissociation have been entirely driven by natural processes. In marine sediments, most gas hydrate within the gas hydrate stability zone is thought to form slowly from dissolved phase methane over thousands to millions of years [*Buffett and Zatsepina*, 2000; *Nimblett and Ruppel*, 2003]. Dissociation of such hydrate may occur slowly (e.g., in response to climate change) or rapidly (e.g., due to the migration of warm fluids or initiation of a submarine slide) and over very small to global length scales, depending on the nature of the forcing process.

[3] Recent years have seen the completion of a few short-term field tests and planning for more extensive tests to assess the viability of producing methane from gas hydrate [e.g., *Boswell et al.*, 2007; *Kurihara et al.*, 2008]. Most production scenarios [e.g., *Collett*, 2002] involve dissociation of natural gas hydrate to extract the methane, and nearly all production methods could lead to inadvertent formation or reformation of gas hydrate within the sediments. Conventional hydrocarbon exploration and production can also lead to hydrate dissociation when warm fluids are pumped through the hydrate stability zone. The length and time scales for hydrate dissociation and formation related to either conventional production or production from gas hydrates are much smaller than those involved in a global warming event such as the Late Paleocene Thermal Maximum [e.g., *Dickens et al.*, 1995]. Yet the impact of anthropogenic activities on natural gas hydrates ultimately requires closer attention owing to the potential for jeopardizing the infrastructure associated with the production itself.

[4] Hydrate formation or dissociation is accompanied by pronounced volume changes, as can be inferred by comparing the density of water (1000 kg m^{-3}) to that of methane hydrate (910 kg m^{-3}). A given volume of water expands 26% upon combining with methane to form Structure I methane hydrate. If methane hydrate dissociates at constant pressure of 10 MPa, the combined volume occupied by the compressed gas and water will be 2.62 times larger than the initial volume of hydrate [*Kwon et al.*, 2008]. Rapid dissociation might accompany production by thermal stimulation and will cause a very large increase in pore fluid pressure and a corresponding decrease in effective stress and shear strength under undrained conditions, as can be seen in numerical modeling results [*Rutqvist et al.*, 2009]. Such a scenario would create high-pressure gradients that will drive fluid flow and trigger fluid flow localization.

[5] While there have been some focused laboratory efforts [e.g., *Watanabe et al.*, 2006], no study has ever systematically documented the volume changes associated with hydrate formation and dissociation in different soils, at a range of effective stress, and for hydrate saturations ranging from 0% to 100% of pore space. This study seeks to fill this gap by measuring the volume change associated with formation and dissociation of tetrahydrofuran (THF) hydrate, which is fully miscible in water. The lack of a gas phase in our experiments allows us to isolate the impact of the hydrate formation and dissociation alone and to develop a mechanistic understanding of the impact of these phase transformations on sediment properties. Further experiments will be required to document the impact of gas release on sediment volume during the dissociation of representative natural hydrates although we present some reasoning about the expected consequences of such dissociation.

2. Laboratory Experiments

[6] Experiments were conducted in a zero–lateral strain cell instrumented to measure the one-dimensional volume change and the compressibility of sediments with or without hydrate. The cell had inner diameter of 100.6 mm and height of 80 mm. The specimen height was limited to 40–50 mm to ensure optimal conditions for oedometric measurements. More details about the cell are given by J. Y. Lee et al. (Parametric study of the physical properties of hydrate-bearing sand, silt, and clay: 1. Electromagnetic properties, submitted to *Journal of Geophysical Research*, 2009) and *Lee* [2007]. A K-type thermocouple mounted through the top cap of the cell monitored the specimen temperature with a precision of 0.1°C. Volume change was determined from the instantaneous vertical position of the porous top cap using a linear variable displacement transducer (LVDT) with precision of 2.5×10^{-6} m. Volume change was measured during loading at

constant temperature and at constant load during hydrate formation and dissociation (changing temperature). The cell, the loading frame, and peripheral electronics were operated in a cold room, where the temperature was controlled with precision of 0.01°C.

[7] We tested specimens made of sand (uniform, round, quartz particles; 120 μm mean grain size; specific surface ~0.02 m^2g^{-1}), crushed silica flour silt (angular particles, 20 μm mean grain size; specific surface ~0.11 m^2g^{-1}), precipitated silica flour silt (each grain is an aggregation of smaller particles with an interparticle porous networks; 20 μm mean aggregate size; specific surface ~120 m^2g^{-1}), and kaolinite clay (platy particles; 1.1μm mean size; specific surface ~36 m^2g^{-1}). Details and photomicrographs of the soils are provided by *Yun et al.* [2007].

[8] The hydrate former for this study is tetrahydrofuran (THF), a clear, colorless, low-viscosity organic compound (C_4H_8O). *Lee et al.* [2007] provide a detailed discussion of the advantages and the disadvantages of using THF as hydrate former. THF is characterized by high volatility, a low freezing point (−108.5°C), and complete miscibility with water. THF forms structure II hydrate, and THF hydrate formation from stoichiometric solution is accompanied by theoretical volume expansion of 7.4%. At a THF to water molar ratio of 1:17, which corresponds to a volume fraction of 21.0% THF and 79.0% water, all pore fluid is converted to hydrate, producing a hydrate volume fraction of S_{hyd} = 1.0. To obtain S_{hyd} = 0.5, we choose a pore fluid mixture consisting of 10.5% THF and 89.5% water, which produces excess water (not excess THF) after hydrate formation. It should be noted that THF hydrate, unlike natural gas hydrate, does not dissociate to both gas (hydrate former) and liquid (water).

[9] We tested specimens with a target S_{hyd} of 0, 0.5, and 1. In each case, the soil specimens were first thoroughly saturated with water (for S_{hyd} = 0) or with the premixed THF-water solution. The specimens were prepared very rapidly to minimize selective evaporation of THF. More details about measures taken to avoid evaporation with THF solutions are given by *Lee et al.* [2007] and *Yun et al.* [2007]. After the cell was filled with the sediment-liquid mixture, it was placed in the loading frame ready to start the test.

[10] Following sample preparation, an external load was applied to the specimen without hydrate. The specimen was then allowed to consolidate until excess pore fluid pressure dissipated and vertical deformation ceased. We then lowered the temperature to induce hydrate formation by cooling to −1°C to −4°C, followed by a 1 day stabilization period at 0.5°C. The specimen with target S_{hyd} = 0.5 required very slow cooling to prevent ice formation, yielding very long duration experimental tests of several days per cycle. Following hydrate formation, the cold room temperature was increased to trigger dissociation of S_{hyd} = 0.5 samples, while the cell temperature was increased with cold room temperature held constant at 10°C to cause dissociation of the S_{hyd} = 1.0 samples. The duration of the dissociation event was hours for the S_{hyd} = 1.0 samples and days for the S_{hyd} = 0.5 samples. A new load was applied following dissociation. These steps were repeated for the vertical effective stress levels σ'_v of 0.01, 0.1, 0.5, and 1.2 MPa. After the final cycle of loading and hydrate formation, the hydrate-bearing specimens were unloaded to simulate core extraction in the field.

3. Experimental Results

[11] The void ratio signatures recorded during the loading-formation-dissociation cycles at σ'_v of 0.01, 0.1, 0.5, and 1.2 MPa are given in Table 1 and shown in Figure 1 (sand), Figure 2 (crushed silt), Figure 3 (kaolinite clay) and Figure 4 (precipitated silt). Void ratio e is related to porosity n through $n/(1-n)$. For sand, precipitated silt, and clay, we conducted experiments at S_{hyd} = 0.5 and S_{hyd} = 1.0, but only S_{hyd} = 1.0 was used for the crushed silt experiments, which were not originally part of our comprehensive study of the physical properties of hydrate-bearing sediments [e.g., *Cortes et al.*, 2009; *Lee*, 2007; *Santamarina and Ruppel*, 2008; *Yun et al.*, 2007; Lee et al., submitted manuscript, 2009; J. Y. Lee et al., Parametric study of the physical properties of hydrate-bearing sand, silt, and clay: 2. Small-strain mechanical properties, submitted to *Journal of Geophysical Research*, 2009].

[12] Overall, the results show that void ratio changes during consolidation, hydrate formation, and hydrate dissociation are much smaller in sediments with low specific surface and rigid granular skeletons (sands) than in normally consolidated sediments with high specific surface and soft skeletons (clays). Hydrate formation to intermediate volume fraction (S_{hyd} = 0.5) causes contraction in all soils, but hydrate formation to high volume fraction (S_{hyd} = 1) is accompanied by volume expansion for low effective stress. Dissociation of THF hydrate,

Table 1. Test Data[a]

Soil	S_s (m^2/g)	S_{hyd}	C_c	C_s	σ'_v (MPa)	Void Ratio		
						Consolidation	Formation	Dissociation
Sand	0.019	0.5	0.03	0.01	0.01	0.591	0.589	0.587
					0.10	0.572	0.570	0.569
					0.51	0.547	0.545	0.544
					1.21	0.535	0.536	na
		1.0	0.04	0.01	0.01	0.595	0.595	0.595
					0.10	0.594	0.594	0.594
					0.51	0.568	0.567	0.566
					1.21	0.544	0.543	na
Crushed silt	0.113	1.0	0.12	0.03	0.01	0.770	0.812	0.777
					0.10	0.728	0.747	0.718
					0.51	0.668	0.667	0.657
					1.21	0.603	0.600	na
Clay	36.5	0.5	0.22	0.04	0.01	0.971	0.895	0.872
					0.10	0.731	0.655	0.642
					0.51	0.562	0.563	0.547
					1.21	0.483	0.486	na
		1.0	0.20	0.02	0.01	0.814	0.861	0.738
					0.10	0.641	0.672	0.599
					0.51	0.502	0.526	0.479
					1.21	0.424	0.457	na
Precipitated silt	120	0.5	2.2	0.12	0.01	6.761	6.662	6.400
					0.10	5.888	5.972	5.769
					0.51	4.334	4.396	4.254
					1.21	3.465	3.529	na
		1.0	1.6	0.05	0.01	5.678	5.908	5.469
					0.10	4.771	5.118	4.602
					0.51	3.708	3.944	3.592
					1.21	3.128	3.180	na

[a]The abbreviation na means not available.

which does not release gas, is always accompanied by some contraction, regardless of stress level or soil.

[13] Figure 5 shows the evolution of void ratio in the standard e versus $\log(\sigma'_v/1\ \text{kPa})$ diagram during a loading-formation-dissociation cycle. The void ratio follows the normal consolidation line during loading, either increases or decreases during hydrate formation, and systematically falls below the normal consolidation line during dissociation. When the load is increased again, the trend of void ratio versus $\log(\sigma'_v/1\ \text{kPa})$ again evolves toward the normal consolidated line. However, the formation-dissociation cycle may have permanently altered the soil fabric, and additional loading does not necessarily erase the effects of the previous thermal cycle. Similar observations were made in frozen ground by *Nixon and Morgenstern* [1973].

[14] The normal consolidation line and the lines that connect void ratios at the end of formation and dissociation converge at high vertical effective stress, implying smaller freeze-thaw changes in void ratio at higher effective stress levels (Figures 5a and 5b). Frozen ground studies show that these lines converge in clays at the void ratio that corresponds to the shrinkage limit [*Chamberlain and Gow*, 1979]. The asymptotic decline in void ratio changes at high effective stress during either formation or dissociation of hydrate has been recently corroborated by our laboratory in a study of hydrate-free and synthetic hydrate-bearing sands that were recovered from hydrate-bearing units at Milne Point on the Alaska North Slope (S. Dai et al., Mount Elbert sediments (with and without hydrates): Characteristics, mechanical properties and geophysical parameters, submitted to *Marine and Petroleum Geology*, 2009).

[15] The change in void ratio Δe after a formation-dissociation cycle scales with the sediment compressibility and is inversely proportional to the stress that is applied during the formation-dissociation cycle. The reduction in void ratio during a complete formation-dissociation cycle can be as high as the change in void ratio due to doubling the effective stress. The sediment compressibility is characterized by the compression index C_c, which is defined as the slope of the compression line on a plot of void ratio versus the log of vertical effective stress,

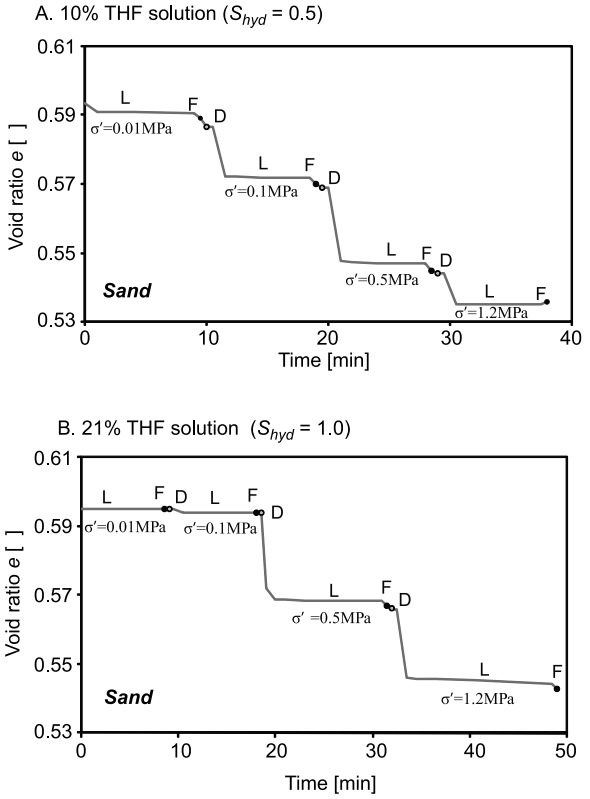

Figure 1. Volume changes induced by loading (L), hydrate formation (F), and hydrate dissociation (D) in sand specimens. (a) The 10% THF solution (S_{hyd} = 0.5 after hydrate formation). (b) The 21% THF solution (S_{hyd} = 1.0 after hydrate formation).

$C_c = \Delta e/\Delta(\log[\sigma'_v/1\ \text{kPa}])$. Values of the compression index reported in Table 1 are computed using changes in void ratio between σ'_v = 0.1 MPa and 1.2 MPa.

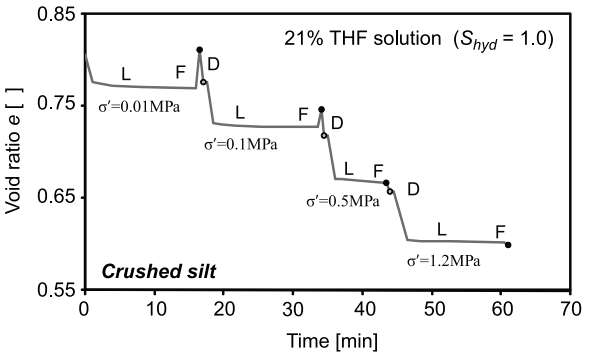

Figure 2. Volume changes in crushed silt specimens. Labeling is the same as in Figure 1. In this case, experiments were completed only with a 21% THF solution, corresponding to S_{hyd} = 1.0 after hydrate formation. Formation and dissociation times are several hours.

[16] The volumetric strain ε_{vol} experienced by the samples can be expressed as $\varepsilon_{vol} = \Delta e/(1 + e_0)$, where e_0 and Δe denote the original void ratio and the change in void ratio, respectively. Between σ'_v = 0.01MPa and σ'_v = 1.2MPa, ε_{vol} for the water saturated samples is ~0.04 in sand, ~0.1 in crushed silt, 0.2 in kaolinite, and 0.5 in precipitated silt. Values of ε_{vol} and by extension C_c rank according to specific surface.

4. Discussion

[17] This section discusses the similarities and differences between frozen ground and hydrate-bearing sediments, with particular focus on a comparison between the most important microscale processes in each system. We also describe microscale hydrate formation and dissociation mechanisms that explain the experimentally observed changes in specimen volume and explore the issue of dissociation settlement, which has profound importance for the integrity of boreholes and

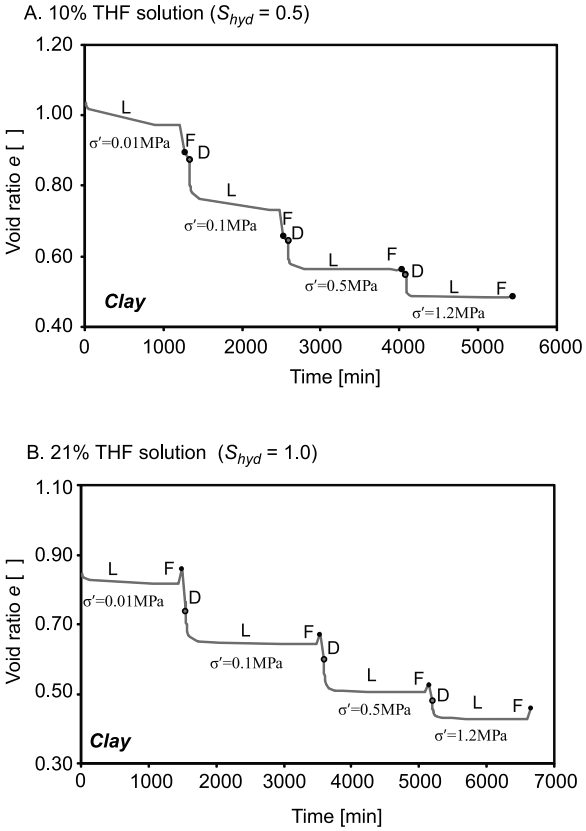

Figure 3. Volume changes in clay specimens. Labeling is the same as in Figure 1. (a) The 10% THF solution (S_{hyd} = 0.5 after hydrate formation). (b) The 21% THF solution (S_{hyd} = 1.0 after hydrate formation).

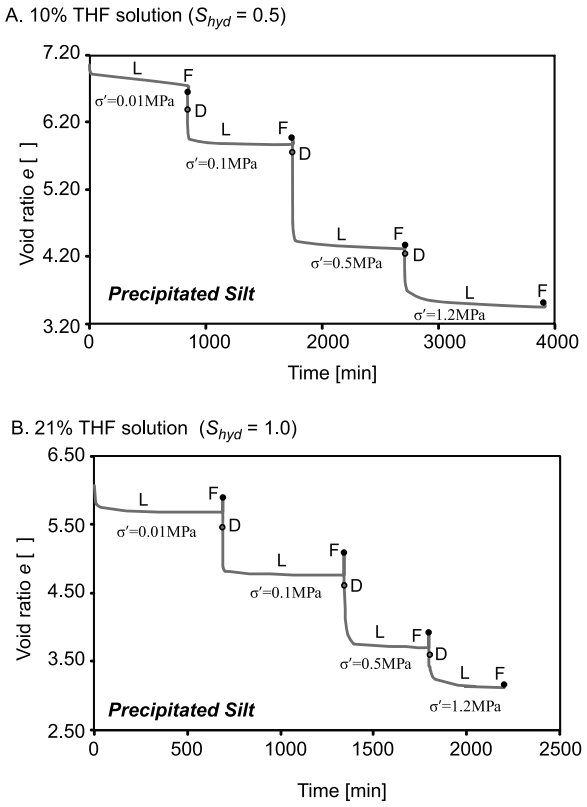

Figure 4. Volume changes in precipitated silt specimens. Labeling is the same as in Figure 1. (a) The 10% THF solution (S_{hyd} = 0.5 after hydrate formation). (b) The 21% THF solution (S_{hyd} = 1.0 after hydrate formation).

infrastructure in the vicinity of gas hydrate production wells.

4.1. Frozen Ground and Hydrate-Bearing Sediments

[18] Three primary volume change phenomena occur in the formation of ice-bearing soils (frozen ground): volume expansion during freezing, cryogenic suction (in fine grained sediments), and segregation of the liquid phase to form ice lenses. Such phenomena have long been expected to occur during hydrate formation as well [e.g., *Clennell et al.*, 1999], and our results highlight some important similarities and differences between hydrate-bearing and ice-bearing systems. First we review fundamental observations associated with the formation of frozen ground.

4.1.1. Key Results of Frozen Ground Engineering

[19] Pore volume expansion associated with ice formation causes water expulsion if drained conditions prevail, as is the case when the ice growth rate is slower than the rate of pore pressure dissipation [*McRoberts and Morgenstern*, 1975]. Ice fills the larger pores first, while unfrozen water remains in the smaller pores. Ice growth is energetically preferred over nucleation at new sites, so that water migrates toward the existing ice phase causing negative pore pressure, higher effective stress, and overconsolidation of the nearby sediment [*Chamberlain and Gow*, 1979; *Konrad and Morgenstern*, 1982]. This describes the phenomenon of cryogenic suction.

[20] In fine grained soils, water expulsion dominates at initial stages of freezing, and suction becomes dominant later. The transition from expulsion to suction is governed by the overburden pressure and the sediment type [*Konrad and Morgenstern*, 1982]. Therefore, expansion is not a linear function of the ice volume fraction. In fact, sediment expansion is only observed when the ice content exceeds a critical value, which can be as high as 85% [*Michalowski and Zhu*, 2006].

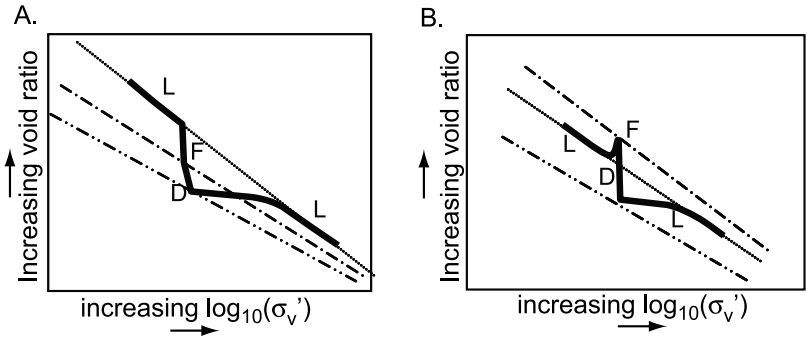

Figure 5. Schematic summary of volume change results during the formation of disseminated hydrate from a dissolved phase hydrate former and during dissociation under drained conditions. (a) Low S_{hyd} and (b) high S_{hyd} and low effective stress.

[21] The magnitude of cryogenic suction is related to the curvature of the ice-water interface, which is a function of the pore size [*Holden et al.*, 1981]. The soil skeleton expands only when the pressure in the ice due to capillary action exceeds the overburden pressure plus the pressure required to initiate grain separation. High overburden pressure reduces the capacity of the soil skeleton to expand upon freezing under drained conditions.

[22] Under some conditions, volume expansion and the associated changes in hydraulic conduction cause a positive feedback loop that leads to the formation of ice lenses. This phenomenon occurs in fine-grained soils subjected to a burial depth at which the effective stress is lower than the capillary pressure the ice experiences. Ice lenses form in the horizontal direction, normal to the geothermal freezing front. Vertical ice-filled cracks often found in frozen ground are not lenses per se, but rather shrinkage cracks that formed as a result of cryogenic suction and contraction of the soil mass [*Chamberlain and Gow*, 1979].

[23] All soils contract upon thawing of ice, even when the effective stress is kept constant. If lenses are present, then the estimates of contraction must take into account the volume of the lenses. In more homogeneous ice-bearing soils, contraction during thawing reflects overconsolidation and particle rearrangement that occurs by cryogenic suction during freezing [*Chamberlain and Gow*, 1979]. For sediments harboring dispersed ice, the volumetric strain associated with thawing ε_{vol}^{thaw} increases as the mass density of the frozen ground ρ_{frozen} decreases according to an empirical equation of the form:

$$\varepsilon_{vol}^{thaw} = A - 0.868\sqrt{\frac{\rho_{frozen}}{\rho_{water}} - 1.15} \pm 0.05, \qquad (1)$$

where A is 0.9 for low-plasticity clays and 0.8 for silts and clay-rich soils with $\rho_{frozen}/\rho_{water}$ of 1.2 to 2.0 [*Nixon and Ladanyi*, 1978; *Watson et al.*, 1973]. This empirical relationship inherently considers the soil mineralogy and specific surface as well as the effective stress at the time of ice formation. While equation (1) could be extended to hydrate-bearing sediments, the data on which it is based are derived from near-surface soils, low–effective stress conditions, and full water-ice transformation. An appropriate expression for hydrate-bearing sediments is obtained in section 4.4.

[24] After a freeze-thaw cycle, sediment permeability is higher, even though the porosity has decreased [*Chamberlain and Gow*, 1979; *Konrad and Samson*, 2000]. The increase in permeability is associated with the development of preferential flow planes in response to lensing and freezing-induced fabric rearrangements.

[25] In summary, effective stress, the rate of cooling, pore size distribution, and the hydraulic conductivity determine volume expansion upon cooling as well as the formation of lenses in frozen ground [*Nixon*, 1991].

4.1.2. Differences Between Ice and Hydrate Formation in Sediments

[26] One of the key differences between the formation of ice and hydrate in sediments is the degree of volume expansion expected in each case under unconfined conditions. Water volume expansion upon freezing is 9%. By the time a mass of water has accepted all of the needed methane molecules to fully convert into Structure I hydrate with all available cages filled, the initial volume of the water has increased by 26%. For our experiments, THF is fully soluble in water, and there are two alternatives: (1) If the experiment is initiated with a stoichiometric solution, water experiences a volume expansion of 7.4% when it converts into hydrate, close to the volume change associated with the water to ice transformation, and (2) if the experiment is initiated with a given mass of water and THF molecules are added until all the water forms hydrate, the initial volume of water expands 36%, which more closely resembles the volume change associated with the formation of methane hydrate. In this study, we designed experiments to be consistent with the first alternative, meaning that our study of volume changes with hydrate formation yields more conservative results than would be expected had hydrate been formed from methane.

[27] The arguments about volume change can be reversed to explain ice melting and hydrate dissociation. Melting of ice liberates water at a lower volume than hydrate dissociation. CH_4 hydrate dissociation not only liberates water, but also gas (assuming constant fluid pressure) at a much higher volume. The miscibility of THF means that the dissociation of THF hydrate produces a water-THF solution and volume contraction.

[28] Another key difference between ice and hydrate formation is the limiting factor for its growth. Ice formation is obviously water limited, but hydrate formation is likely to be mostly limited by the availability of methane (in aqueous or gaseous phase) except in rare cases [e.g., *Liu and Flemings*,

2006]. In typical frozen ground settings, most of the available water will form ice, particularly in coarse-grained sediments. This means that it is impossible to study frozen ground for conditions in which only a fraction of the pore water has formed ice. The amount of water that is bound into hydrate at a given location can range from 0% to 100%, depending on the availability of the hydrate former and other factors. Therefore, our experiments enforce a THF-limited situation that permits us to control S_{hyd}. Both ice and hydrate formation are restricted by capillary effects (e.g., *Clennell et al.* [1999] for hydrates) and ion exclusion.

[29] Lenses are common features in both ice- and hydrate-bearing sediments. Hydrate lenses interpreted as primary features (not features produced as a consequence of the stress release, fluid flow, and hydrate dissociation associated with conventional coring) have now been described in a variety of sediments and in both passive and active margin hydrate provinces [e.g., *Holland et al.*, 2008; *Trehu et al.*, 2004]. Ice lenses are largely restricted to a subhorizontal orientation, consistent with the typical geothermal field having isotherms oriented subparallel to the ground surface. This orientation restriction disappears in hydrate-bearing sediments, where fluid/gas migration and/or the stress field gain relevance in defining the orientation of lensing. In our laboratory experiments, we closely controlled the effective stress and operated under drained conditions, with no gas phase present. Thus, we obtained a relatively homogeneous distribution of hydrate in the sediments [*Lee et al.*, 2007].

4.2. Hydrate Formation

[30] Competing mechanisms deform sediments and therefore determine the net volume change during hydrate formation (Figure 6). At low hydrate saturation (approximately $S_{hyd} < 0.25$), hydrate grows inside a pore and can cause an increase in pore pressure and a decrease in the effective stress under undrained conditions. Typically, water advection controls the availability of methane. Thus, the rate of hydrate formation is lower than the rate of pore pressure dissipation in natural sediments, and there is no increase in fluid pressure or decrease in effective stress until S_{hyd} exceeds ~0.6. With increasing hydrate concentration ($0.25 < S_{hyd} < 0.6$), the growing crystals can push against neighboring mineral grains and trigger the buckling of skeletal force chains, leading to sediment contraction.

[31] At high hydrate saturation ($S_{hyd} > \sim 0.7$), many pores become occluded, the hydraulic conductivity decreases, and methane transport could become diffusion dominated. Cryogenic suction causes negative fluid pressure, an increase in effective stress, and the consolidation of the sediment around the growing hydrate mass. The whole sediment mass expands to reflect volume expansion in the hydrate mass working against the effective confining stresses.

4.3. Hydrate Dissociation

[32] Based on the previous discussion, it follows that the volume change during dissociation at constant fluid pressure and effective stress should be small if the initial hydrate saturation is below the hydrate skeleton interaction limit, perhaps $S_{hyd} \leq 0.5$. On the other hand, if the initial hydrate saturation exceeds ~0.5, dissociation alters the force equilibrium at the particle scale, and volume contraction should be expected, as shown in Figure 6b.

[33] Hydrate formation from dissolved phase methane within the hydrate stability zone in marine sediments is believed to be a relatively slow process. In contrast, dissociation due to either natural or man-made events can occur rapidly and lead to a pronounced increase in fluid pressure and decrease in effective stress. Such changes are in part due to skeletal contraction effects that were discussed above and that are common to ice, THF hydrate, and methane hydrate. However, for methane hydrate dissociation, the most important impact we anticipate is very substantial accompanying fluid expansion. Based on the approach of *Kwon et al.* [2008], a volume V_0 of methane hydrate expands to occupy a volume $2.62V_0$ at a constant pressure of 10 MPa, with water volume of $0.79V_0$ and gas volume of $1.83V_0$.

4.4. Dissociation Settlement

[34] Soil settlement upon melting of frozen ground (thaw settlement) is a well-known phenomenon that has a substantial impact on infrastructure [e.g., *Andersland and Ladanyi*, 2003; *Nelson et al.*, 2001; *Pullman et al.*, 2007]. The potential for settlement of soils upon hydrate dissociation is a largely unstudied phenomenon that could affect borehole stability, foundation settlement and ground subsidence around a production well. Four causes of bulk volume change during hydrate dissociation can be identified: (1) sediment softening and volume contraction ε_{vol}^{thaw} due to hydrate dissociation at constant effective stress, (2) the van-

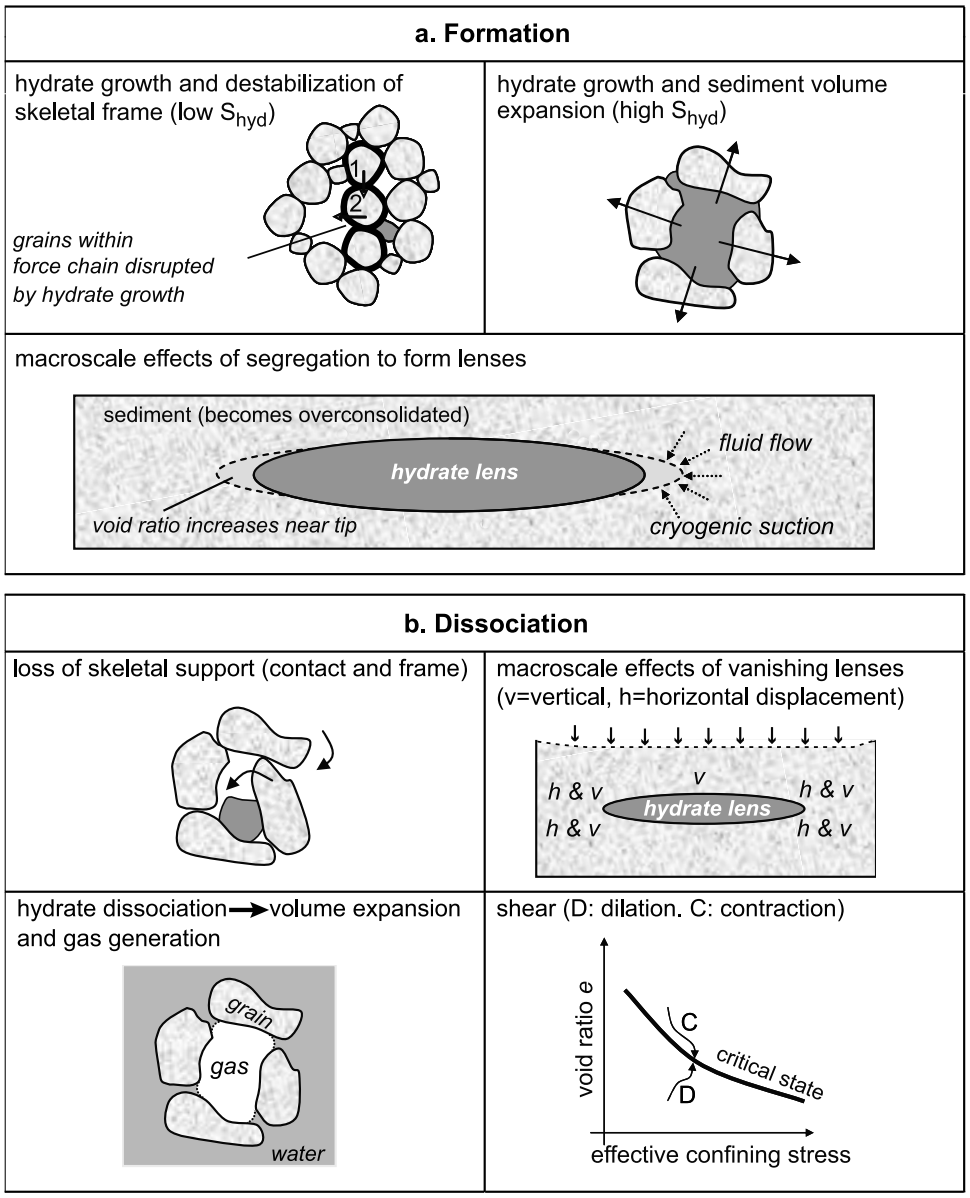

Figure 6. Pore and particle-scale processes during hydrate formation and dissociation from a fully miscible, dissolved phase hydrate former. Individual sediment grains are shown in the gray pattern, while dark gray denotes gas hydrate in all cases. Arrows shown associated with individual grains denote displacement of the grains due to the specific hydrate-related process described in each case.

ishing of the segregated hydrate volume ε_{vol}^{lens} in lenses and nodules, (3) additional volume change in the sediment without hydrate ε_{vol}^{ps} associated with a chosen production strategy, and (4) volume contraction or dilation if the sediment is subjected to marked deviatoric loading ε_{vol}^{q}. The expansion transient that may take place during thermal stimulation is not included in this analysis, but should be recognized whenever the rate of volume expansion is higher than the flow rate, as could be the case in fine grained sediments.

4.4.1. Dissociation at Constant Effective Stress ε_{vol}^{thaw}

[35] Volumetric strains during hydrate dissociation $\varepsilon_{vol}^{thaw} = (e_F - e_D)/(1 + e_F)$ are plotted versus compression index in Figure 7 for all specimens, hydrate saturations, and stress conditions. In view of the limited amount of available data and their variability, we can only propose an upper bound expression for the volumetric strain during hydrate dissociation in terms of the two controlling vari-

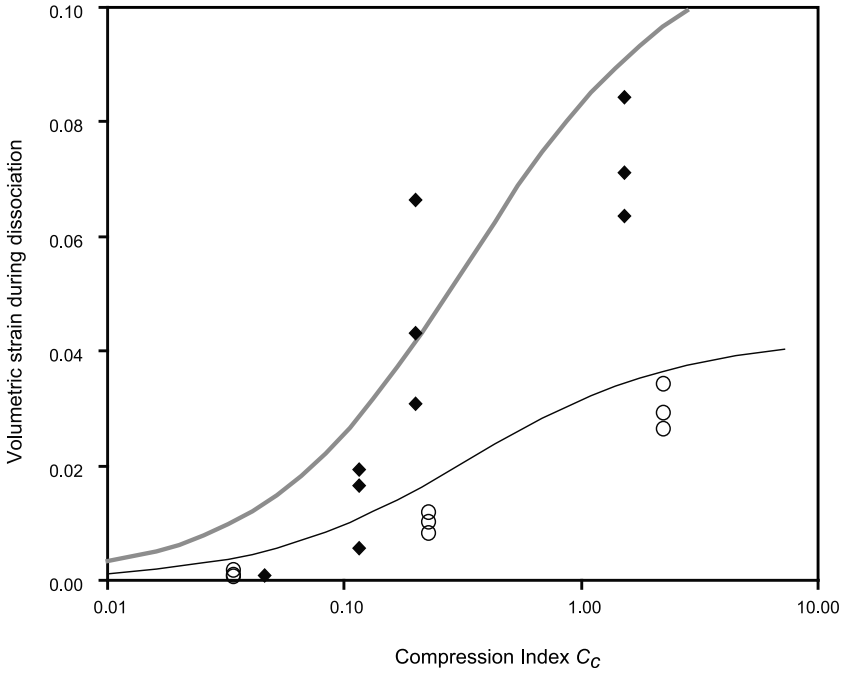

Figure 7. Contractive volumetric strain during THF hydrate dissociation (produces no gas) in sediments. Solid symbols correspond to S_{hyd} = 1.0, and open circles represent data for S_{hyd} = 0.5. Gray and black curves denote the upper bounds from equation (2) for the S_{hyd} = 1.0 and S_{hyd} = 0.5 samples, respectively.

ables, hydrate fraction S_{hyd} and sediment compressibility C_c:

$$\varepsilon_{vol}^{thaw} \leq \frac{S_{hyd}^{1.4}}{3} \frac{C_c}{1+3C_c}. \quad (2)$$

This hyperbolic expression applies to 18 of the 19 measured data points and properly captures the early increase in volumetric strain with sediment compressibility C_c and the diminishing volumetric strain increases at high C_c values. The asymptotic value in (2) is ε_{vol}^{thaw} = 1/9 or ~10%. The exponent 1.4 on S_{hyd} underscores the fact that dissociating THF hydrates have only a very small effect on volume change for low S_{hyd}.

4.4.2. Vanishing of Segregated Hydrate ε_{vol}^{lens}

[36] The dissociation of lenses and nodules is followed by a complex sequence of events that involves fluid volume expansion, drainage and cavity closure, and interaction among lenses. The simplest estimation function for engineering design can take a linear form

$$\varepsilon_{vol}^{lens} = \beta V_{lens}, \quad (3)$$

where V_{lens} is the volume fraction of segregated hydrate, and β is a factor that depends on the size and orientation of the segregated hydrate masses and that takes into account soil arching. We can anticipate that $\beta \approx 1$ for horizontal lenses of large areal extent, and $\beta < 1$ for vertical lenses and nodules. Appropriate values of β can be inferred from numerical modeling that takes into consideration the constitutive parameters of the surrounding sediment.

4.4.3. Volume Change ε_{vol}^{ps} Associated With Selected Production Methods

[37] Thermal stimulation, depressurization, chemical inhibition, and replacement of methane by other gases have been proposed as production strategies to recover methane from natural hydrates [*Collett*, 2002; *Graue et al.*, 2006; *Holder et al.*, 1984; *McGrail et al.*, 2004]. All these mechanisms cause volume change in sediments without hydrates, particularly in fine-grained soils [*Mitchell and Soga*, 2005].

[38] Of the four potential production mechanisms, we anticipate that depressurization will have the greatest impact on volume, an inference confirmed by the numerical simulation of *Kimoto et al.* [2007]. Fluid depressurization Δu will cause an increase in effective stress from the in situ value σ'_v to $\sigma'_v + \Delta u$. The associated volumetric strain ε_{vol}^{ps}

can be estimated by taking into consideration the sediment compressibility C_c:

$$\varepsilon_{vol}^{ps} \approx \frac{C_c}{1+e_o}\log\left(\frac{\sigma_v^{'}+\Delta u}{\sigma_v^{'}}\right). \quad (4)$$

4.4.4. Volume Change due to Dissociation Under High Shear ε_{vol}^{q}

[39] Experimental evidence for a wide range of soil processes shows that sediments converge to the critical stress condition when subjected to high shear strain, regardless of differences in thermo-hydromechanical conditions that they have experienced in the past. This is also the case for hydrate bearing sediments [*Hyodo et al.*, 2007; *Yoneda et al.*, 2008]. If the initial volume average void ratio of the hydrate bearing sediment is e_o and the stress-dependent critical state void ratio after dissociation is e_{cs}, the volumetric strain will be:

$$\varepsilon_{vol}^{q} = \frac{e_{cs}-e_o}{1+e_o} = \frac{\left(e_{1kPa}-\lambda\log\frac{p^{'}}{1kPa}\right)-e_o}{1+e_o}, \quad (5)$$

where $e_{1\mathrm{kPa}}$ and λ are the critical state parameters of the sediment and p' is the final mean effective stress after dissociation.

4.4.5. Total Volume Change $\varepsilon_{vol}^{total}$

[40] A simple additive rule is assumed as a first approximation to estimate the total volume contraction $\varepsilon_{vol}^{total}$ upon dissociation under one-dimensional zero–lateral strain boundary conditions:

$$\varepsilon_{vol}^{total} = \varepsilon_{vol}^{thaw} + \varepsilon_{vol}^{lens} + \varepsilon_{vol}^{ps}. \quad (6)$$

Such conditions would apply in the far field near a production well on level ground. On the other hand, only one term is needed to estimate volume change after dissociation if large shear strains are anticipated after hydrate dissociation, such as in sloping ground or beneath footings:

$$\varepsilon_{vol}^{total} = \varepsilon_{vol}^{q}. \quad (7)$$

The value of initial void ratio in equation (5) must be a mesoscale volume average value to take into consideration the presence of segregated hydrate as well.

5. Conclusions

[41] Experimental results were obtained with THF hydrate, which does not produce gas upon dissociation. Differences with methane hydrate bearing sediments should arise when undrained conditions prevail during either formation or dissociation.

[42] Water expands when it combines with a hydrate former to produce hydrate, but the growth of disseminated hydrate in pores causes no significant volume change under drained conditions (e.g., common in coarse-grained sediments in nature) when the hydrate saturation is low. In fact, irreversible fabric changes and cryogenic suction during early hydrate growth cause volume contraction, probably until S_{hyd}~0.5. Expansion during hydrate formation takes place when the hydrate saturation is high (probably S_{hyd} greater than ~0.7) and the effective stress is low.

[43] Volume change during dissociation under high shear is determined by the initial volume average void ratio and the stress-dependent critical state void ratio of the sediment.

[44] Hydrate dissociation under zero lateral strain, drained conditions is accompanied by sediment contraction in all sediments for all effective stress levels and hydrate saturation values. The volumetric strain scales with the sediment compressibility C_c and the hydrate volume fraction $S_{hyd}^{1.4}$.

[45] Besides sediment volume contraction due to the dissociation of disseminated hydrate, two other causes for volume contraction are identified during hydrate dissociation under zero lateral strain conditions: (1) the vanishing of segregated hydrate (e.g., lenses and nodules) and (2) the contraction of the sediment mass due to selected production strategy, particularly when depressurization is used.

Acknowledgments

[46] This research was initially supported by the Chevron Joint Industry Project on Methane Hydrates under contract DE-FC26-01NT41330 from the U.S. Department of Energy to Georgia Tech. Additional support was provided to J. Y. Lee by KIGAM, GHDO, and MKE and J. C. Santamarina by the Goizueta Foundation. C. Ruppel thanks the USGS Gas Hydrates Project and the MIT Earth Resources Laboratory for providing logistical support for completion of this work. Comments from W. Waite, T. Kneafsey, and an anonymous reviewer and successive insightful reviews by N. Sultan improved the manuscript. Any use of a trade, product, or firm name is for descriptive purposes only and does not imply endorsement by the U.S. Government. Any opinions, findings, conclusions, or recommendations expressed herein are those of the authors and do not necessarily reflect the view of the DOE or the USGS.

References

Andersland, O. B., and B. Ladanyi (2003), *Frozen Ground Engineering*, 363 pp., John Wiley, New York.

Boswell, R., T. S. Collett, S. A. Digert, R. B. Hunter, and S. Hancock (2007), Gas hydrate investigations at the 2007 Mount Elbert test site, Milne Point area, Alaska North Slope, *Eos Trans. AGU*, *88*(52), Fall Meet. Suppl., Abstract OS21A-02.

Buffett, B., and O. Zatsepina (2000), Formation of gas hydrate from dissolved gas in natural porous media, *Mar. Geol.*, *164*, 69–77, doi:10.1016/S0025-3227(99)00127-9.

Chamberlain, E. J., and A. J. Gow (1979), Effect of freezing and thawing on the permeability and structure of soils, *Eng. Geol.*, *13*, 73–92, doi:10.1016/0013-7952(79)90022-X.

Clennell, M. B., M. Hovland, J. S. Booth, P. Henry, and W. J. Winters (1999), Formation of natural gas hydrates in marine sediments: 1. Conceptual model of gas hydrate growth conditioned by host sediment properties, *J. Geophys. Res.*, *104*, 22,985–23,303, doi:10.1029/1999JB900175.

Collett, T. S. (2002), Energy resource potential of natural gas hydrate, *AAPG Bull.*, *86*, 1971–1992.

Cortes, D., A. I. Martin, T. S. Yun, F. M. Francisca, J. C. Santamarina, and C. Ruppel (2009), Thermal conductivity of hydrate-bearing sediments, *J. Geophys. Res.*, *114*, B11103, doi:10.1029/2008JB006235.

Dickens, G. R., J. R. O'Neil, D. K. Rea, and R. M. Owen (1995), Dissociation of oceanic methane hydrate as a cause of the carbon isotope excursion at the end of the Paleocene, *Paleoceanography*, *10*, 965–971, doi:10.1029/95PA02087.

Graue, A., B. Kvamme, B. A. Baldwin, J. Stevens, J. Howard, E. Aspenese, G. Ersland, J. Husebo, and D. Zornes (2006), CO_2 storage in natural-gas-hydrate reservoirs benefits from associated methane production, *JPT J. Pet. Technol.*, *58*, 65–67.

Holden, J. T., R. H. Jones, and S. J. M. Dudek (1981), Heat and mass flow associated with a freezing front, *Eng. Geol.*, *18*, 153–164, doi:10.1016/0013-7952(81)90055-7.

Holder, G. D., V. A. Kamath, and S. P. Godbole (1984), The potential of natural gas hydrates as an energy resource, *Annu. Rev. Energy*, *9*, 427–445, doi:10.1146/annurev.eg.09.110184.002235.

Holland, M., P. Schultheiss, J. Roberts, and M. Druce (2008), Observed gas hydrate morphologies in marine sediments, paper presented at the 6th International Conference on Gas Hydrates, Chevron, Vancouver, B. C., Canada, 6–10 July.

Hyodo, M., Y. Nakata, N. Yoshimoto, and R. Orense (2007), Shear behavior of methane hydrate-bearing sand, paper presented at the Seventeenth International Offshore and Polar Engineering Conference, Int. Soc. of Offshore and Polar Eng., Lisbon, Portugal, July 1–6.

Kimoto, S., F. Oka, T. Fushita, and M. Fuiwaki (2007), A chemo-thermo-mechanically coupled numerical simulation of the subsurface ground deformation due to methane hydrate dissociation, *Comput. Geotech.*, *34*, 216–228, doi:10.1016/j.compgeo.2007.02.006.

Konrad, J.-M., and N. R. Morgenstern (1982), Effects of applied pressure on freezing soils, *Can. Geotech. J.*, *19*, 494–505, doi:10.1139/t82-053.

Konrad, J.-M., and M. Samson (2000), Influence of freezing temperature on hydraulic conductivity of silty clay, *J. Geotech. Geoenviron. Eng.*, *126*, 180–187, doi:10.1061/(ASCE)1090-0241(2000)126:2(180).

Kurihara, M., et al. (2008), Analysis of the JOGMEC/NRCan/Aurora Mallik gas hydrate production test through numerical simulation, paper presented at the 6th International Conference on Gas Hydrates, Chevron, Vancouver, B. C., Canada, 6–10 July.

Kwon, T. H., G. C. Cho, and J. C. Santamarina (2008), Gas hydrate dissociation in sediments: Pressure temperature evolution, *Geochem. Geophys. Geosyst.*, *9*, Q03019, doi:10.1029/2007GC001920.

Lee, J. Y. (2007), Hydrate-bearing sediments: Formation and geophysical properties, Ph.D. dissertation, 226 pp.,Ga. Inst. of Technol., Atlanta.

Lee, J. Y., T. Yun, J. C. Santamarina, and C. Ruppel (2007), Observations related to tetrahydrofuran and methane hydrates for laboratory studies of hydrate-bearing sediments, *Geochem. Geophys. Geosyst.*, *8*, Q06003, doi:10.1029/2006GC001531.

Liu, X., and P. B. Flemings (2006), Passing gas through the hydrate stability zone at southern Hydrate Ridge, offshore Oregon, *Earth Planet. Sci. Lett.*, *241*, 211–226, doi:10.1016/j.epsl.2005.10.026.

McGrail, B. P., T. Zhu, R. B. Hunter, M. B. White, S. L. Patil, and A. S. Kulkarni (2004), A new method for enhanced production of gas hydrates with CO_2, paper presented at Hedberg Conference, Am. Assoc. of Pet. Eng., Vancouver, B. C., Canada.

McRoberts, E. C., and N. R. Morgenstern (1975), Pore water expulsion during freezing, *Can. Geotech. J.*, *12*, 130–141, doi:10.1139/t75-012.

Michalowski, R. L., and M. Zhu (2006), Frost heave modeling using porosity rate function, *Int. J. Numer. Anal. Methods Geomech.*, *30*, 703–722, doi:10.1002/nag.497.

Mitchell, J. K., and K. Soga (2005), *Fundamentals of Soil Behavior*, 577 pp., John Wiley, New York.

Nelson, F. E., O. A. Anisimov, and N. I. Shiklomanov (2001), Subsidence risk from thawing permafrost, *Nature*, *410*, 889–890, doi:10.1038/35073746.

Nimblett, J., and C. Ruppel (2003), Permeability evolution during the formation of gas hydrates in marine sediments, *J. Geophys. Res.*, *108*(B9), 2420, doi:10.1029/2001JB001650.

Nixon, J. F. (1991), Discrete ice lens theory for frost heave in soils, *Can. Geotech. J.*, *28*, 843–859, doi:10.1139/t91-102.

Nixon, J. F., and B. Ladanyi (1978), Thaw consolidation, in *Geotechnical Engineering for Cold Regions*, edited by O. B. Andersland and D. M. Anderson, chap. 4, pp. 164–215, McGraw-Hill, New York.

Nixon, J. F., and N. R. Morgenstern (1973), The residual stress in thawing soils, *Can. Geotech. J.*, *10*, 571–580, doi:10.1139/t73-053.

Pullman, E. R., M. T. Jorgenson, and Y. Shur (2007), Thaw settlement in soils of the Arctic Coastal Plain, Alaska, *Arct. Antarct. Alp. Res.*, *39*, 468–476, doi:10.1657/1523-0430 (05-045)[PULLMAN]2.0.CO;2.

Rutqvist, J., G. J. Moridis, T. Grover, and T. Collett (2009), Geomechanical response of permafrost-associated hydrate deposits to depressurization-induced gas production, *J. Pet. Sci. Eng.*, *67*, 1–12.

Santamarina, J. C., and C. Ruppel (2008), The impact of hydrate saturation on the mechanical, electrical, and thermal properties of hydrate-bearing sand, silts, and clay, paper presented at the 6th International Conference Gas Hydrates, Chevron, Vancouver, B. C., Canada, 6–10 July.

Trehu, A. M., et al. (2004), Three-dimensional distribution of gas hydrate beneath southern Hydrate Ridge: Constraints from ODP Leg 204, *Earth Planet. Sci. Lett.*, *222*, 845–862, doi:10.1016/j.epsl.2004.03.035.

Watanabe, K., K. Yokokawa, and Y. Muto (2006), Observation of frost heave of THF clathrate hydrate on porous glass powder, in *Current Practices in Cold Regions Engineering* [CD-ROM], edited by M. Davis and J. E. Zufelt, doi:10.1061/40836(210)44, Am. Soc. of Civ. Eng., Reston, Va.

Watson, G. H., W. A. Slusarchuk, and R. K. Rowley (1973), Determination of some frozen and thawed properties of permafrost soils, *Can. Geotech. J.*, *10*, 592–606, doi:10.1139/t73-055.

Yoneda, J., M. Hyodo, Y. Nakata, and N. Yoshimoto (2008), Time-dependent elasto-plastic constitutive equation for sedimentary sands supported by methane hydrate, paper presented at the 12th Japan Symposium on Rock Mechanics and the 29th Western Japan Symposium on Rock Engineering, Jpn. Comm. for Rock Mech., Ube, Japan, 2–4 Sept.

Yun, T. S., J. C. Santamarina, and C. Ruppel (2007), Mechanical properties of sand, silt, and clay containing tetrahydrofuran hydrate, *J. Geophys. Res.*, *112*, B04106, doi:10.1029/2006JB004484.